Reducing the Inductors of Rectifiers Having Two Outputs to Improve Power Density

Qing-Chang Zhong, *Fellow, IEEE*, and Wen-Long Ming, *Member, IEEE*

***Abstract*—In this paper, a recently reported single-phase rectifier with two outputs (RECTO) is improved to reduce the neutral inductor and the grid inductor, by moving the neutral inductor away from the path of the grid current. The neutral inductor does not carry the grid current any more so the current stress of the neutral inductor can be significantly reduced, and the size of the inductor becomes much smaller. In theory, the current stress can be reduced by at least three times and the size of the inductor can be reduced by nine times. At the same time, the grid inductor can be reduced to achieve the same level of grid-current switching ripples because of the changed operation modes and modulation strategy. Together, the reduced neutral and grid inductors help improve the system power density. It is worth noting that the voltage and current stresses of the switches and the other features of the RECTO, e.g., two dc outputs and unity power factor, are not affected. Comparative experimental results are presented to demonstrate the reduction. If the two load currents are the same then the neutral inductor is only required to handle the switching ripples. This improved RECTO is particularly suitable for applications with two balanced loads without increasing the cost much.**

***Index Terms*—Current stress, grid inductor, neutral inductor, power density, single-phase rectifier with two outputs, switching ripple.**

I. Introduction

TO DATE , single-phase rectifiers have been widely used in ac and dc microgrids [1], [2]. During the last few years, the increasingly growing problems caused by burning fossil fuels have considerably advanced the development of microgrids and also the single-phase rectifiers [1], [3]–[5], which play an important role in microgrids. The generic function of rectifiers is to convert ac voltages to dc voltages and also to control the power exchanged between the ac and dc sides. One application for such rectifiers is to provide two independent dc outputs from one ac input. For example, many electronic systems need positive and negative dc power suppliers at the same time [6]. As a popular solution, half-bridge rectifiers are very attractive because they can provide two dc voltage outputs at relatively low costs [7]. However, the performance of half-bridge rectifiers could be degraded because of two main drawbacks. One is the limited range of the two dc outputs, which are dependent on each other and also on system parameters, such as loads, capacitors and the source voltage [7]. This can be partly solved through injecting dc currents [8] or adding auxiliary circuits [9]–[11] at the ac or dc sides. However, these solutions suffer from high dc bias in the grid current, low input power factor and/or limited voltage regulation range determined by the ratio of the dual loads. Another drawback is that bulky dc capacitors are often inevitable in half-bridge rectifiers, which are used to level and smooth the voltage ripples caused by charging and discharging the capacitors to provide the grid current. However, this could lead to significantly reduced power density, which is unacceptable for volume-critical and/or weight-critical systems like electrical vehicles and aircraft power systems [12]–[15].

As reported in [6] and [16], the single-phase rectifier with two outputs (in short, RECTO, for simplicity) shown in Fig. 2, which is formed by adding an independently controlled neutral leg [1], [17], [18] into conventional half-bridge rectifiers, was proposed to overcome the two aforementioned drawbacks. A typical application of RECTO is shown in Fig. 1, which can provide two separate voltage outputs with the presence of a neutral line so that it is possible to power loads at three different voltage levels [11]. It is worth highlighting that the RECTO has two independent outputs so it does allow a single load to be operated. Hence, the applications cover both single and double loads. Thanks to the independently controlled neutral leg, the two dc voltage outputs become independent from each other and also robust against parameter variations in loads and capacitors. Moreover, the dc capacitors required are significantly reduced because the grid current is diverted away from the split capacitors and flows through the neutral leg.

Apart from the four switches and the two dc capacitors, there are another two components in the conventional RECTO, i.e., the grid inductor L_g and the neutral inductor L_N, as shown in Fig. 2. The inductor L_g is connected to the grid, which should be large enough to limit the switching ripples of the grid current for power quality [19], [20]. On the other hand, the inductor L_N is used for the control of the two independent voltage outputs. The current flowing through the neutral inductor L_N is the sum of the grid current and the current difference of the dual loads, which can be high. Hence, the size of this inductor can be very large, leading to low power density.

In this paper, the grid and neutral inductors are reduced by proposing an improved RECTO to reduce the current stress of

Manuscript received June 16, 2016; revised October 4, 2016; accepted November 19, 2016. Date of publication December 6, 2016; date of current version May 9, 2017. Recommended for publication by Associate Editor J.-I. Itoh.

Q.-C. Zhong is with the Department of Electrical and Computer Engineering, Illinois Institute of Technology, Chicago, IL 60616 USA (e-mail: zhongqc@ieee.org).

W.-L. Ming is with the School of Engineering, Cardiff University, Cardiff CF24 3AA, U.K. (e-mail: wenlongming@gmail.com).

Color versions of one or more of the figures in this paper are available online at http://ieeexplore.ieee.org.

Digital Object Identifier 10.1109/TPEL.2016.2636219

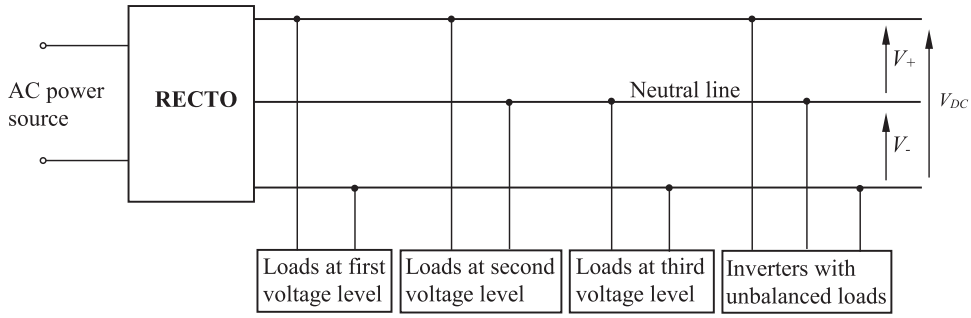

Fig. 1. Typical application of the RECTO.

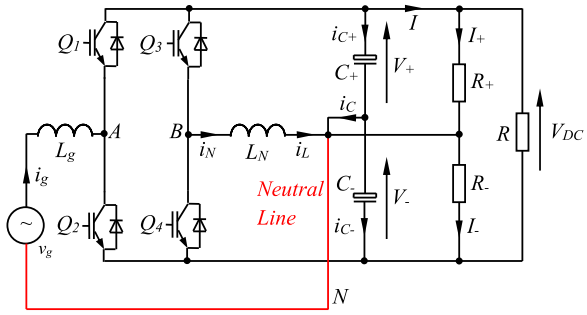

Fig. 2. RECTO presented in [6].

the neutral inductor L_N and the switching ripples of the grid current. In the improved RECTO, the neutral inductor L_N is moved away from the path of the grid current so L_N only carries the current difference of the dual loads, without the grid current. Since the maximum value of the current difference is often much smaller than that of the grid current, the current stress of the neutral inductor can be significantly reduced. Accordingly, the size of the inductor becomes much smaller. Theoretically, the current stress can be reduced by at least three times and the inductor size by at least nine times. It is worth highlighting that the reduction can be always achieved, which does not depend on a specific system design and/or system parameters. In order to further demonstrate the reduction, a numerical example, together with experimental validation, are presented. It is found that, in the given example system, the current stress is reduced by about 25 times. The reduction of current stress can be different if system parameters are changed but at least three times can be always achieved. The operation modes and modulation strategy of the improved RECTO are changed, which help reduce the minimum inductance of the grid inductor L_g for the same switching ripple. As a result, the system power density is further improved. Additionally, the voltage, current stress of switches, and the other functions of the conventional RECTO, e.g., two dc outputs and the unity power factor, are not affected. It is worth mentioning that the leakage current of the proposed RECTO becomes higher compared to that of the conventional RECTO because of the neutral inductor. Instead of being directly connected together, the neutral line is now connected to the midpoint of the dc side through the neutral inductor, which is similar to that in conventional full-bridge rectifiers. In this case, the proposed RECTO is more suitable for applications, where the common-mode electromagnetic interference (EMI) is not an important issue or effective methods have been applied to suppress the EMI.

Compared to [21], the new contributions in this paper mainly include the following:

1) the reduction of the neutral inductor current is systematically analyzed through theoretical and experimental comparison;
2) it is revealed and experimentally verified that the improved RECTO is also able to reduce the switching ripple in the grid current while the same grid inductor is used;
3) the pulse width modulation (PWM) strategy and operation principles of the improved RECTO are given;
4) a detailed comparison is made on the neutral inductors, grid inductors, and power semiconductor switches between the conventional and improved RECTO.

The rest of this paper is organized as follows. In Section II, the derivation of the improved RECTO is given. After that, the operation principles, models and modulation strategy of the improved RECTO are discussed in Section III. Then, Section IV is devoted to the control design of the improved RECTO. In order to clearly show the improvement, a comparison is made between the conventional and improved RECTO in Section V. Finally, experimental results are given in Section VI with conclusions made in Section VII.

II. Improved RECTO

Same as the conventional RECTO proposed in [6] and [16], the improved RECTO also has two legs, i.e., the rectification leg and the neutral leg. Instead of connecting the neutral line N to the midpoint of the split capacitors, as shown in Fig. 2, the neutral line N in the improved RECTO is connected to the midpoint of the two switches in the neutral leg, as shown in Fig. 3. The rectification leg consists of switches Q_1 and Q_2 and the inductor L_g, whereas the neutral leg consists of switches Q_3 and Q_4, the inductor L_N and the split capacitors C_+ and C_-. The input of the rectifier is the grid voltage v_g and the outputs are two dc voltages V_+ and V_-. Three loads R, R_+, and R_- can be operated at the same time. Since the two dc outputs are independent from each other, there are no restrictions on the ratio among the loads, which means the loads can be the same or different, as the conventional RECTO proposed in [6] and [16]. The two legs are still operated independently from each other. The rectification leg is operated as a single-phase half-bridge rectifier with Q_1 and Q_2 operated in a complementary manner

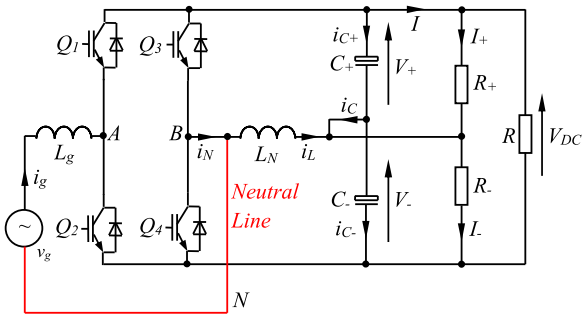

Fig. 3. Proposed improved RECTO.

TABLE I
OPERATION MODES

Mode	Q_1	Q_2	Q_3	Q_4	$v_{\rm AN}$
1	0	1	0	1	0
2	1	0	0	1	$V_{\rm DC}$
3	1	0	1	0	0
4	0	1	1	0	$-V_{\rm DC}$

to track the reference grid current, which is often set to be in phase with the grid voltage to achieve the unity power factor. The neutral leg is operated as a dc/dc converter to control the two dc outputs and to provide the return path of the grid current.

Although only the neutral line is slightly moved, it helps reduce the switching ripple of the grid current and also divert the grid current away from the neutral inductor L_N. As a result, the current stress of the inductor L_N can be significantly reduced. The maximum current carried by L_N can be reduced by at least three times; see Section V for detailed analysis with a numerical example. Importantly, all the main functions of the conventional RECTO are not affected so the grid current can be well controlled and the two dc outputs are still independent from each other.

III. Circuit Analysis

A. Operation Modes

According to the ON and OFF states of the four switches, there are four different operation modes, as summarized in Table I and shown in Fig. 4, where the solid lines indicate the paths that carry currents and the dashed lines indicate the paths that do not carry currents. In Mode 1 and Mode 3, the voltage between points A and N, i.e., $v_{\rm AN}$, is 0. On the other hand, the voltage $v_{\rm AN}$ is $V_{\rm DC}$ and $-V_{\rm DC}$ in Mode 2 and Mode 4, respectively. It should be mentioned that currents can flow through either the diodes or the transistors of switches. For example, in Mode 1, the positive half cycle of the grid current flows through the transistor of switch Q_2 and the diode of the switch Q_4, whereas the negative half cycle of the grid current flows through the transistor of switch Q_4 and the diode of switch Q_2.

B. Average Circuit Model

Assume the grid voltage is

$$v_g = V_g \sin \omega t. \tag{1}$$

The grid current with the unity power factor can be given as

$$i_g = I_g \sin \omega t \tag{2}$$

where V_g, I_g, and ω are the peak value of the grid voltage, peak value of the grid current, and the angular line frequency, respectively. Following the procedures mentioned in [2], [6], and [7], the average circuit model of the improved RECTO can be built, as shown in Fig. 5. Switches Q_1 and Q_3 are replaced by current sources, whereas switches Q_2 and Q_4 are replaced by voltage sources. In the average circuit model, d_1, d_2, d_3, and d_4 are the duty cycles of the switches Q_1, Q_2, Q_3, and Q_4, respectively. Note that $d_1 + d_2 = 1$ and $d_3 + d_4 = 1$ because the two switches of each leg are operated complementarily.

According to the average circuit model, the equivalent circuit of the improved RECTO in voltage sources are shown in Fig. 6. Since the voltages across the inductors L_g and L_N are much lower than the voltages V_+, V_-, and $V_{\rm DC}$, these voltages are neglected in order to simplify the analysis. As a result

$$-V_{\rm DC} d_1 + V_g \sin \omega t + V_- = 0 \tag{3}$$

$$-V_{\rm DC} d_2 + V_+ - V_g \sin \omega t = 0 \tag{4}$$

$$V_{\rm DC} d_3 = V_- \tag{5}$$

$$V_{\rm DC} d_4 = V_+ \tag{6}$$

according to Kirchhoff's voltage law, which means

$$d_1 = \frac{V_-}{V_{\rm DC}} + \frac{V_g}{V_{\rm DC}} \sin \omega t \tag{7}$$

$$d_2 = \frac{V_+}{V_{\rm DC}} - \frac{V_g}{V_{\rm DC}} \sin \omega t \tag{8}$$

$$d_3 = \frac{V_-}{V_{\rm DC}} \tag{9}$$

$$d_4 = \frac{V_+}{V_{\rm DC}}. \tag{10}$$

In the improved RECTO, the voltages V_+, V_-, and $V_{\rm DC}$ are used to supply dc loads so they are expected to be dc with low ripples. In order to satisfy $d_1 > 0$ and $d_2 > 0$

$$V_- > V_g \tag{11}$$

$$V_+ > V_g \tag{12}$$

and

$$V_{\rm DC} = V_+ + V_- > 2V_g. \tag{13}$$

The conditions (11), (12), and (13) are the basic principles to operate the improved RECTO.

However, according to (7)–(10), there are no restrictions on the relationship between V_+ and V_-. As a result, V_+ can be higher, equal, or lower than V_- without any restrictions, which means that they are fully independent from each other.

C. Modulation Strategy

The circuit waveforms of the improved RECTO are shown in Fig. 7(a)–(e). The voltage $v_{\rm AN}$ of the conventional RECTO

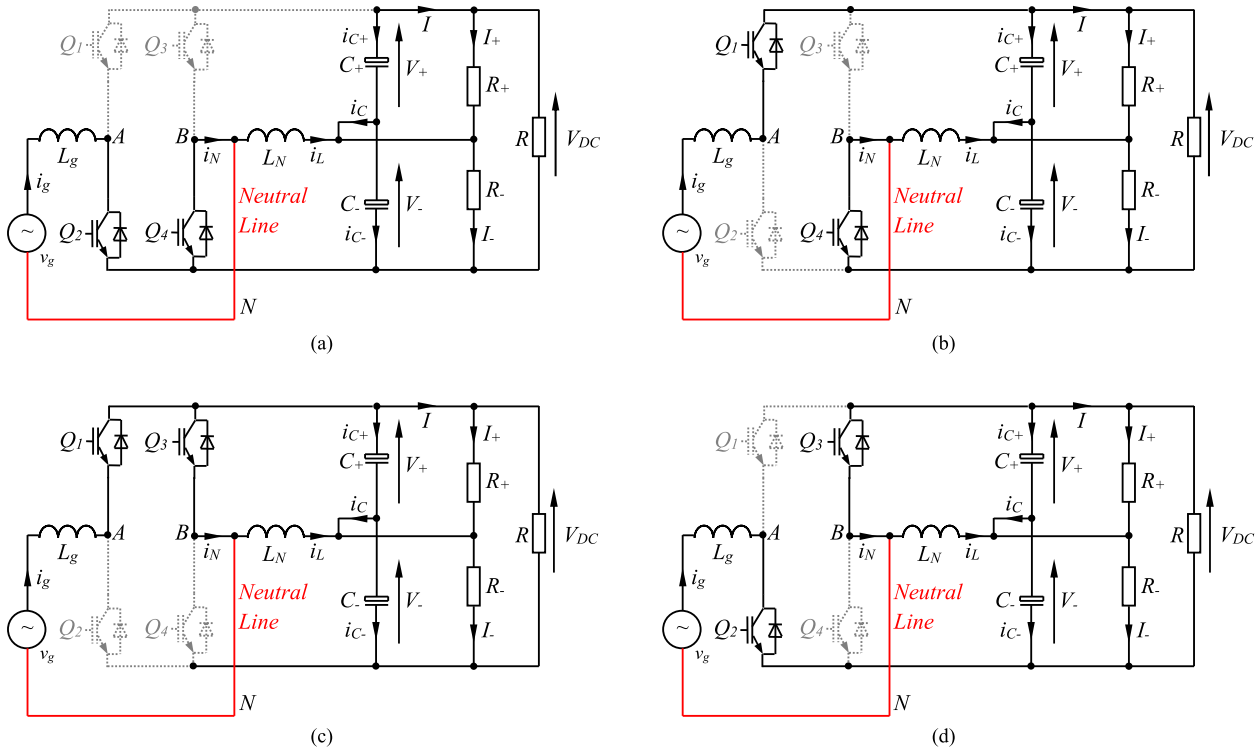

Fig. 4. Operation modes of the improved RECTO: (a) Mode 1 ($v_{\rm AN} = v_{\rm AB} = 0$); (b) Mode 2 ($v_{\rm AN} = v_{\rm AB} = V_{\rm DC}$); (c) Mode 3 ($v_{\rm AN} = v_{\rm AB} = 0$); and (d) Mode 4 ($v_{\rm AN} = v_{\rm AB} = -V_{\rm DC}$).

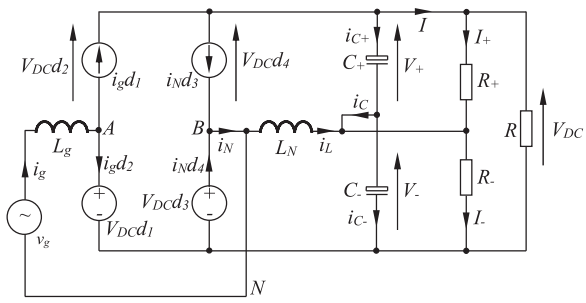

Fig. 5. Average circuit model of the improved RECTO.

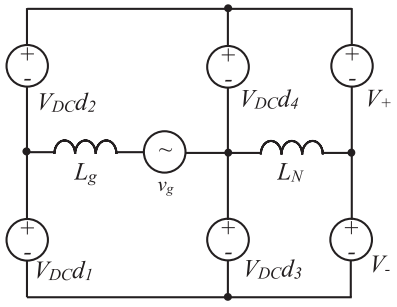

Fig. 6. Equivalent circuit of the improved RECTO in voltage sources.

is shown in Fig. 7(f) for comparison. Switches Q_1 and Q_2 are operated according to the duty cycle d_1 and switches Q_3 and Q_4 are operated according to the duty cycle d_3. According to (7) and (9), the dc components in d_1 and d_3 are the same. The only difference is that there is a fundamental ac component in d_1. Hence, d_1 is always higher than d_3 in the positive half cycle of d_1 and always lower than d_3 in the negative half cycle of d_1. As a result, the ON time of switch Q_1 is always longer than that of switch Q_3 in the positive half cycle. On the other hand, theON time of Switch Q_3 is always longer than that of Switch Q_1 in the negative half cycle. Hence, Mode 4 and Mode 2 do not appear in the positive and negative half cycles, respectively. During the positive half cycle, the circuit operates in the sequence of "Mode 1, Mode 2, Mode 3, and Mode 2," and the voltage $v_{\rm AN}$ rotates in the sequence of "0, $V_{\rm DC}$, 0 and $V_{\rm DC}$." Accordingly, the grid current i_g is increased when $v_{\rm AN} = 0$ and decreased when $v_{\rm AN} = V_{\rm DC}$, as shown in Fig. 7(d). During the negative half cycle, the circuit operates in the sequence of "Mode 4, Mode 1, Mode 4, and Mode 3," and the voltage $v_{\rm AN}$ accordingly rotates in the sequence of "$-V_{\rm DC}$, 0, $-V_{\rm DC}$, and 0". The resulting grid current is decreased and increased when $v_{\rm AN} = 0$ and $v_{\rm AN} = -V_{\rm DC}$, respectively. Clearly, the states with $v_{\rm AN} = -V_{\rm DC}$ and $v_{\rm AN} = V_{\rm DC}$ do not exist in the positive and negative half cycles, respectively, and the voltage $v_{\rm AN}$ in the improved RECTO is unipolar, which helps reduce the switching ripples of the grid current. Note that the same triangle signal is used to generate the gate signals according to d_1 and d_3.

For the conventional RECTO shown in Fig. 2, it is operated as a half-bridge rectifier plus a dc–dc converter. In this case, the voltage $v_{\rm AN}$ changes between V_+ and $-V_-$ according to the ON and OFFstates of switches Q_1 and Q_2, which is not affected by switches Q_3 and Q_4. As shown in Fig. 7(f), $v_{\rm AN} = V_+$ when switch Q_1 is ON and $v_{\rm AN} = -V_-$ when switches Q_2 is ON. As a result, the $v_{\rm AN}$ in the conventional RECTO is bipolar.

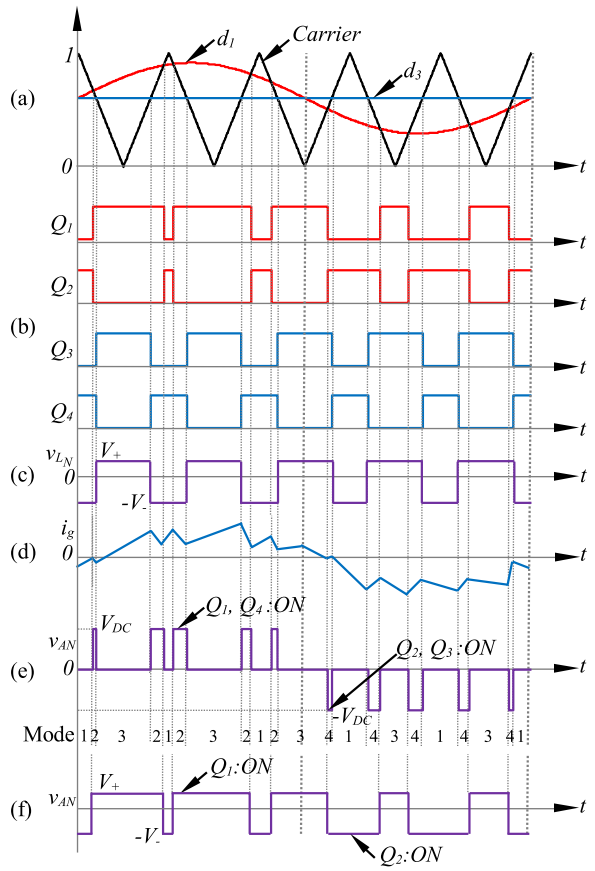

Fig. 7. Operation of the improved and conventional RECTO: (a) carrier, duty cycles d_1 and d_3; (b) drive signals of switches Q_1, Q_2, Q_3, and Q_4; (c) voltage across the inductor L_N, denoted as v_{L_N}, in the improved RECTO; (d) grid current i_g in the improved RECTO; (e) voltage $v_{\rm AN}$ in the improved RECTO; and (f) voltage $v_{\rm AN}$ in the conventional RECTO.

On average, the generated $v_{\rm AN}$ is same for the two RECTO for the same duty cycles. In this case, the average grid current at the fundamental frequency and the dc output voltages are same for both RECTO. However, the obviously different switching operation modes of the two RECTO result in reduced switching ripples of the grid current in the improved RECTO. This will be discussed in detail in Section V.

IV. Control Design

In the improved RECTO, there are four controlled variables, i.e., the grid current i_g, dc voltages V_+ and V_-, and the current i_C. The rectification leg is mainly responsible for controlling the grid current i_g and maintaining the dc bus voltage $V_{\rm DC}$, i.e., the sum of V_+ and V_-; the neutral leg is mainly responsible for splitting the sum $V_{\rm DC}$ and also minimizing the current i_C, which diverts the fundamental current away from inductor L_N.

A. Control of the Rectification Leg

In order to control the dc bus voltage $V_{\rm DC}$, the two dc voltages V_+ and V_- are measured and added together to form $V_{\rm DC}$, before passing through the low-pass filter (LPF)

$$H(s) = \frac{1 - e^{-Ts/2}}{Ts/2} \tag{14}$$

where T is the fundamental period of the grid voltage, to filter out low-frequency and switching-frequency ripples so that the grid current reference is clean without noticeable harmonics. As shown in Fig. 8, a proportional-integral (PI) controller is used here to maintain the dc bus voltage, whose reference is set as $V_{\rm DC}^* = V_+^* + V_-^*$. Due to the power balance between the ac and dc sides of the converter, the output of the voltage PI controller is used as the peak value of the grid current reference. At the same time, the phase information of the grid voltage is extracted by a phase-locked loop [22] to make sure that the grid current is in phase with the grid voltage to achieve the unity power factor.

In order to track the generated grid current reference, the left work is to design a current controller. Many current controllers are available, such as hysteresis controllers [23] with a variable switching frequency, proportional-resonant controllers, and repetitive controllers [24] with a fixed switching frequency, can be used. Because of the excellent performance on handling harmonics, the repetitive controller shown in Fig. 8 is used, which is constructed based on a proportional controller $K_{\rm rr}$ and an internal model given by

$$C(s) = \frac{K_{rr}}{1 - \frac{\omega_i}{s+\omega_i} e^{-\tau_d s}} \tag{15}$$

where K_{rr} and τ_d can be designed according to the analysis mentioned in [1] and [24] as

$$\tau_d = \tau - \frac{1}{\omega_i} = 0.0196\,\text{s} \tag{16}$$

$$K_{rr} = \omega_i L_g \tag{17}$$

with $\omega_i = 2550$ and $\tau = 0.02\,\text{s}$ when the system fundamental frequency is $50\,\text{Hz}$. In practice, the gain K_{rr} can be first set at $\omega_i L_g$ and then tuned by trial and error.

B. Control of the Neutral Leg

For the neutral leg, the main task is to split the voltage $V_{\rm DC}$, i.e., to control one of the voltages V_+ and V_-. Here, controlling V_+ is taken as an example. As shown in Fig. 8, the voltage V_+ is measured as a feedback signal and a PI controller is then used to minimize the error between the V_+ and its reference V_+^*.

As mentioned before, another objective of the neutral leg is to divert the fundamental component away from the current i_L so that the current stress of the inductor L_N can be minimized and the voltage ripples in V_+ and V_- can be reduced. According to the average circuit model shown in Fig. 5

$$i_L = -i_C + I_- - I_+. \tag{18}$$

Since I_+ and I_- are dc currents, the diversion of the fundamental component in i_L can be achieved by controlling either i_L itself or i_C. Due to the fact that the maximum value of the i_L is not less than i_C, the current i_C is controlled here so that the current stress on the current sensor can be minimized, which also helps

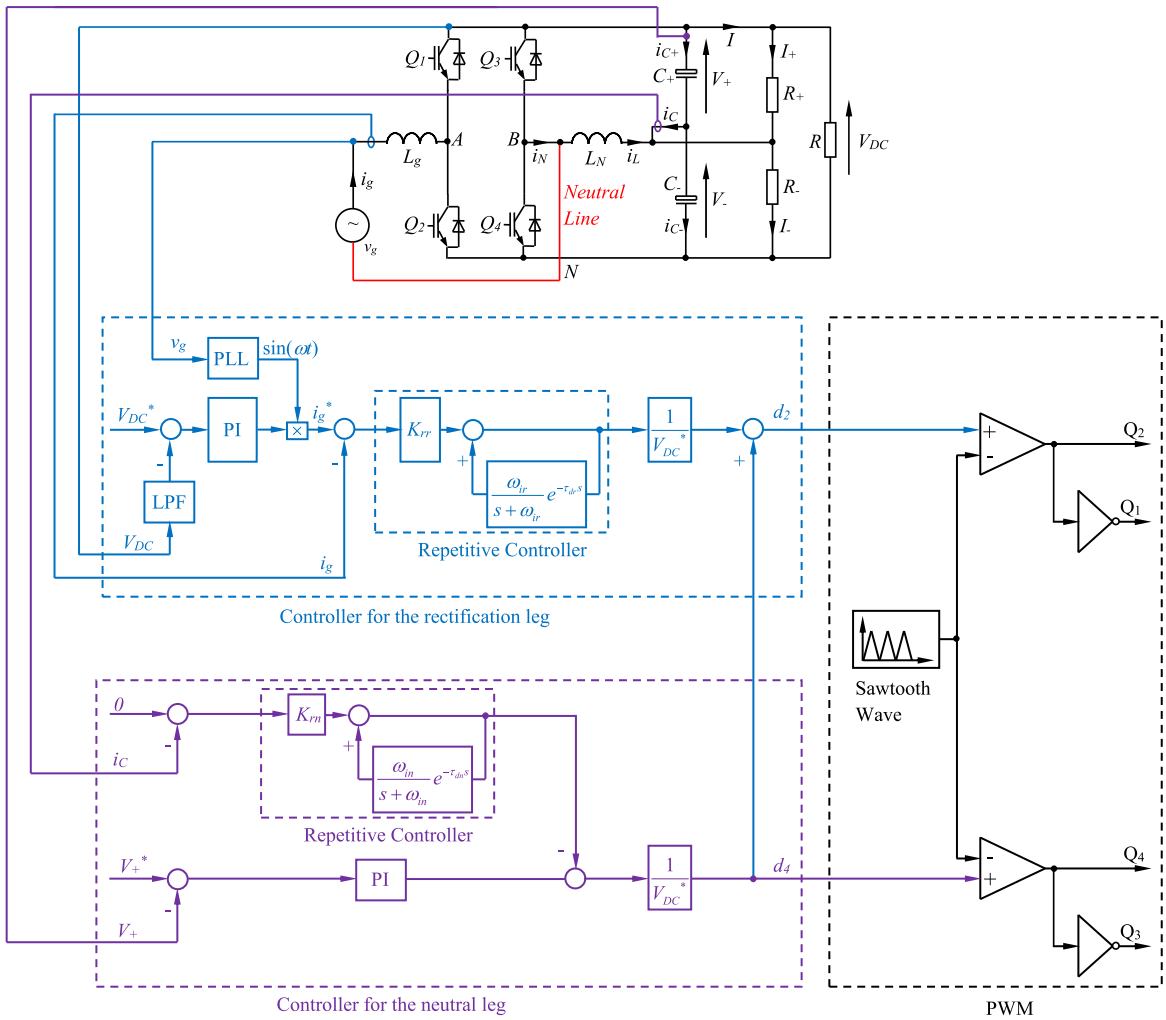

Fig. 8. Controller for the improved RECTO.

reduce system cost in practice. Again, the repetitive current controller used for the rectification leg is adopted to control i_C to be around 0. Hence, all the fundamental current flow through the neutral leg instead of the split capacitors.

The output of the PI controller and the repetitive controller are added together to form the duty cycle d_4. The voltage PI controller is designed to regulate the dc component, whereas the repetitive current controller is designed to deal with the ac fundamental component so that the two loops are decoupled in the frequency domain. In this case, the stability of each loop can be treated individually [1]. As long as each loop is stable, which can be easily guaranteed, the whole control system is stable.

Because of (8), the output d_4 of the controller for the neutral leg is added onto the output of the controller for the rectification leg to produce the duty cycle d_2 for the rectification leg. As shown in Fig. 8, the duty cycles d_2 and d_4 are sent to comparators to generate the drive signals for Q_1, Q_2 and Q_3, Q_4, respectively. Note that the same triangle waveform is used in the two comparators to make sure that the circuit is operated according to the switching pattern shown in Fig. 7. This guarantees that Mode 4 does not appear in the positive half cycle of the grid current and that Mode 3 does not appear in the negative half cycle.

Again, it is worth highlighting that other types of current controllers instead of repetitive controllers can be used in the controllers for both rectification and neutral legs. Hysteresis controllers and proportional-resonant controllers are strong candidates to replace the repetitive controller if needed.

V. Comparison With the Conventional RECTO

In order to facilitate the analysis, V_+, V_-, $V_{\rm DC}$, I_g, I_+, I_-, i_N, i_L, and i_C in the conventional RECTO are denoted as $V_+^{'}$, $V_-^{'}$, $V_{\rm DC}^{'}$, $I_g^{'}$, $I_+^{'}$, $I_-^{'}$, $i_N^{'}$, $i_L^{'}$, and $i_C^{'}$, respectively. V_+, V_-, $V_{\rm DC}$, I_g, I_+, I_-, i_N, i_L, and i_C denote the signals in the improved RECTO.

A. Neutral Inductor L_N

1) Current-Stress Reduction: For the conventional RECTO

$$i_L^{'} = i_N^{'} = I_g^{'} \sin \omega t - i_C^{'} - I_+^{'} + I_-^{'} \tag{19}$$

where $I_+^{'} - I_-^{'}$ is the current difference of the dual loads R_+ and R_-. Because $i_C^{'}$ is controlled around zero, (19) becomes

$$i_L^{'} = I_g^{'} \sin \omega t - I_+^{'} + I_-^{'}. \tag{20}$$

Obviously, $i_L^{'}$ contains a fundamental component $I_g^{'} \sin \omega t$ and a dc component $-I_+^{'} + I_-^{'}$.

For the improved RECTO

$$i_L = i_N - i_g = -i_C - I_+ + I_- \tag{21}$$

where i_C is again controlled around zero, and hence

$$i_L = -I_+ + I_-. \tag{22}$$

It is clear that i_L is a pure dc current without fundamental components.

It is easy to find out that the maximum absolute values of the two inductor currents are

$$|i_L^{'}|_{\max} = I_g + \mid I_+^{'} - I_-^{'} \mid \tag{23}$$

$$|i_L|_{\max} = \mid I_+ - I_- \mid \tag{24}$$

respectively. For a fair comparison, the two RECTO are supposed to operate at the same power level, which means $I_+^{'} = I_+$, $I_-^{'} = I_-$, and $I_g^{'} = I_g$. In this case

$$\frac{|i_L^{'}|_{\max}}{|i_L|_{\max}} = \frac{I_g + \mid I_+^{'} - I_-^{'} \mid}{\mid I_+ - I_- \mid} = 1 + \frac{I_g}{\mid I_+ - I_- \mid}. \tag{25}$$

Because of the power balance between the ac and dc sides of the rectifier

$$\frac{V_g I_g}{2} = V_+ I_+ + V_- I_- + (V_+ + V_-)(I - I_+). \tag{26}$$

Since $V_+ I_+$, $V_- I_-$ and $(V_+ + V_-)(I - I_+)$ are not negative

$$\frac{V_g I_g}{2} \geqslant V_+ I_+ \tag{27}$$

which means

$$\frac{I_g}{I_+} \geqslant \frac{2V_+}{V_g} > 2 \tag{28}$$

because $V_+ > V_g$ in order to ensure the boost operation of the rectifier. Similarly

$$\frac{I_g}{I_-} \geqslant \frac{2V_-}{V_g} > 2. \tag{29}$$

Because of (28) and (29)

$$\frac{|i_L^{'}|_{\max}}{|i_L|_{\max}} = 1 + \frac{I_g}{\mid I_+ - I_- \mid} > 3 \tag{30}$$

is always true. As a result, the maximum current flowing through the inductor L_N is reduced by at least three times in the improved RECTO. The reduced current stress would lower the temperature of the neutral inductor, which helps improve the reliability of the neutral inductor.

Due to the reduced current stress, the inductor size can be accordingly reduced. Since the inductor size is proportionally related to the maximum energy stored in the inductor, if the same inductance L_N is used then the size of the neutral inductor in the improved RECTO can be approximately reduced [25] by at least

$$r_L = \frac{\frac{1}{2} L_N |i_L^{'}|_{\max}^2}{\frac{1}{2} L_N |i_L|_{\max}^2} = \left(\frac{|i_L^{'}|_{\max}}{|i_L|_{\max}} \right)^2 > 9 \tag{31}$$

times. Obviously, the power density of the improved RECTO can be much higher than that of the conventional RECTO.

The reduction ratio $\frac{|i_L^{'}|_{\max}}{|i_L|_{\max}}$ is the ratio of the grid current I_g to the current difference $\mid I_+ - I_- \mid$ plus 1. The higher the ratio, the more the reduction. When the two load currents are balanced, i.e., when $I_+ = I_-$, the current difference is $I_+ - I_- = 0$. In this case, the neutral inductor L_N is only required to handle the switching ripples and can be reduced significantly. In other words, the improved RECTO is particularly suitable for applications with two balanced loads.

2) Selection of the Inductance L_N: Following the procedures in [7], the peak–peak switching ripple of the current i_L can be obtained as

$$\triangle i_L = \frac{V_+ V_-}{L_N f_s V_{\mathrm{DC}}}. \tag{32}$$

If the given maximum switching ripple of the i_L is $\triangle i_{L\max}$, then the required minimum inductance is given as

$$L_{N\min} = \frac{V_+ V_-}{V_{\mathrm{DC}} f_s \triangle i_{L\max}}. \tag{33}$$

The $\triangle i_{L\max}$ is often selected as 20% of the dc component in the current i_L, which is $I_- - I_+$ here.

In order to clearly demonstrate the reduction of the current stress presented above, a numerical example is given here, with the parameters given in Table II. For the references of V_+ and V_- set as 200 V and 250 V, respectively, $I_g = 4.6$ A is used for calculation after considering power losses. The $\triangle i_{\mathrm{Lmax}}$ is selected as 3 A and the resulted minimum inductance L_{Nmin} is 1.9 mH. In practice, a 2.2 mH inductor is used. In addition, the maximum values of the two inductor currents are $|i_L^{'}|_{\max} \approx 4.78$ A and $|i_L|_{\max} \approx 0.18$ A according to (23) and (24), respectively. This represents the reduction of the current

TABLE II
PARAMETERS OF THE SYSTEM

Parameters	Values
Grid voltage (RMS)	110 V
Line frequency	50 Hz
L_g	4.4 mH
L_N	2.2 mH
C_+	1120 μF
C_-	560 μF
R	1470 Ω
R_+	470 Ω
R_-	1000 Ω

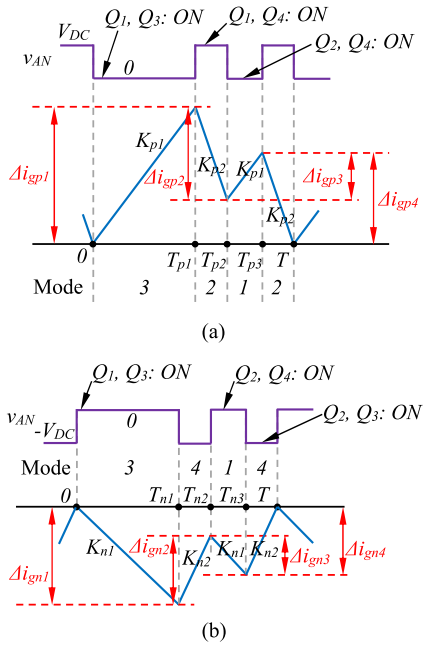

Fig. 9. Grid current i_g and the voltage $v_{\rm AN}$ during a switching period in a (a) positive half cycle and (b) negative half cycle.

stress by $\frac{|i_L'|_{\max}}{|i_L|_{\max}} = \frac{4.78}{0.18} \approx 26$ times, without affecting the current stress of the switches.

B. Grid Inductor L_g

According to the modulation strategy shown in Fig. 7, the waveforms of the voltage $v_{\rm AN}$ and the corresponding grid current i_g are shown in Fig. 9(a) and (b), respectively, for the positive and negative half cycles of the grid current.

1) Switching Ripples of i_g in the Positive Half Cycle: During the positive half cycle, a switching cycle can be divided into the following four parts:

1) during [0, T_{p1}], the grid current i_g increases by $\triangle i_{gp1}$ with the rising rate $K_{p1} = \frac{V_g \sin \omega t}{L_g}$;
2) during [T_{p1}, T_{p2}], the grid current i_g decreases by $\triangle i_{gp2}$ with the falling rate $K_{p2} = \frac{-V_{\rm DC}+V_g \sin \omega t}{L_g}$;
3) during [T_{p2}, T_{p3}], the grid current i_g increases by $\triangle i_{gp3}$ with the rising rate K_{p1};
4) during [T_{p3}, T], the grid current i_g decreases by $\triangle i_{gp4}$ with the falling rate K_{p2}.

Clearly, the four peak–peak values $\triangle i_{gp1}$, $\triangle i_{gp2}$, $\triangle i_{gp3}$, and $\triangle i_{gp4}$ change according to the rising/falling rates and the duty cycles where

$$\begin{aligned} \triangle i_{gp1} &= K_{p1} T_{p1} \\ \triangle i_{gp2} &= -K_{p2}(T_{p2} - T_{p1}) \\ \triangle i_{gp3} &= K_{p1}(T_{p3} - T_{p2}) \\ \triangle i_{gp4} &= -K_{p2}(T - T_{p3}). \end{aligned} \tag{34}$$

According to the PWM operation of the proposed RECTO shown in Fig. 7

$$T_{p1} = \frac{d_3}{f_s} = \frac{V_-}{V_{\rm DC} f_s} \tag{35}$$

$$T_{p3} - T_{p2} = \frac{d_2}{f_s} = \frac{V_+ - V_g \sin \omega t}{V_{\rm DC} f_s}. \tag{36}$$

Since the switching frequency is of several orders compared to the fundamental frequency, the duty cycles d_1, d_2, d_3, and d_4 are constant during a switching period, and the two parts in Mode 2 are approximately equal because of the symmetrical modulating signal. As a result

$$\begin{aligned} T - T_{p3} &= T_{p2} - T_{p1} \\ &= \frac{1 - T_{p1} - (T_{p3} - T_{p2})}{2} \\ &= \frac{1 - d_3 - d_2}{2 f_s} \\ &= \frac{V_g}{2 f_s V_{\rm DC}} \sin \omega t. \end{aligned} \tag{37}$$

Substituting (35), (36), and (37) into (34)

$$\begin{aligned} \triangle i_{gp1} &= \frac{V_- V_g \sin \omega t}{L_g V_{\rm DC} f_s} \\ \triangle i_{gp2} &= \frac{(V_{\rm DC} - V_g \sin \omega t) V_g \sin \omega t}{2 V_{\rm DC} L_g f_s} \\ \triangle i_{gp3} &= \frac{(V_+ - V_g \sin \omega t) V_g \sin \omega t}{V_{\rm DC} L_g f_s} \\ \triangle i_{gp4} &= \frac{(V_{\rm DC} - V_g \sin \omega t) V_g \sin \omega t}{2 V_{\rm DC} L_g f_s}. \end{aligned} \tag{38}$$

The maximum value of $\triangle i_{gp1}$ is given as

$$\triangle i_{gp1\max} = \frac{V_- V_g}{L_g V_{\rm DC} f_s} \tag{39}$$

which is achieved when $\sin \omega t = 1$.

In addition, $\triangle i_{gp2} = \triangle i_{gp4}$. Let $\frac{d \triangle i_{gp2}}{dt} = 0$ and it can be found that, because $V_{\rm DC} > 2V_g$, the maximum value of $\triangle i_{gp2}$ is achieved when $\sin \omega t = 1$ at

$$\triangle i_{gp2\max} = \frac{(V_{\rm DC} - V_g) V_g}{2 V_{\rm DC} L_g f_s}. \tag{40}$$

Similarly, let $\frac{d \triangle i_{gp3}}{dt} = 0$ and the maximum value of the $\triangle i_{gp3}$ can be obtained as

$$\triangle i_{gp3}\max = \frac{(V_+ - V_g) V_g}{V_{\rm DC} L_g f_s} \tag{41}$$

when $V_+ \geqslant 2V_g$, corresponding to $\sin \omega t = 1$, and as

$$\triangle i_{gp3\max} = \frac{V_+^2}{4 V_{\rm DC} L_g f_s} \tag{42}$$

when $V_+ \leqslant 2V_g$, corresponding to $\sin \omega t = \frac{V_+}{2V_g}$.

2) Switching Ripples of i_g in the Negative Half Cycle: Similarly, a switching period in the negative half cycle can be divided into the following four parts:

1) during [0, T_{n1}], the grid current i_g decreases by $\triangle i_{\rm gn1}$ with the falling rate $K_{n1} = \frac{V_g \sin \omega t}{L_g}$;
2) during [T_{n1}, T_{n2}], the grid current i_g increases by $\triangle i_{\rm gn2}$ with the falling rate $K_{n2} = \frac{V_{\rm DC}+V_g \sin \omega t}{L_g}$;
3) during [T_{n2}, T_{n3}], the grid current i_g decreases by $\triangle i_{\rm gn3}$ with the falling rate K_{n1};
4) during [T_{n3}, T], the grid current i_g increases by $\triangle i_{\rm gn4}$ with the rising rate K_{n2}.

Similarly

$$\begin{aligned}\triangle i_{\rm gn1} &= -K_{n1}T_{n1}\\ \triangle i_{\rm gn2} &= K_{n2}(T_{n2}-T_{n1})\\ \triangle i_{\rm gn3} &= -K_{n1}(T_{n3}-T_{n2})\\ \triangle i_{\rm gn4} &= K_{n2}(T-T_{n3})\end{aligned} \tag{43}$$

and

$$\begin{aligned}T_{n1} &= \frac{d_1}{f_s} = \frac{V_- + V_g \sin \omega t}{V_{\rm DC} f_s}\\ T_{n3}-T_{n2} &= \frac{d_4}{f_s} = \frac{V_+}{V_{\rm DC} f_s}\\ T-T_{n3} &= \frac{1-d_1-d_4}{2f_s} = \frac{-V_g \sin \omega t}{2V_{\rm DC} f_s}\\ T_{n2}-T_{n1} &= \frac{1-d_1-d_4}{2f_s} = \frac{-V_g \sin \omega t}{2V_{\rm DC} f_s}.\end{aligned} \tag{44}$$

Substituting (44) into (43)

$$\begin{aligned}\triangle i_{\rm gn1} &= -\frac{(V_- + V_g \sin \omega t)V_g \sin \omega t}{V_{\rm DC} L_g f_s}\\ \triangle i_{\rm gn2} &= -\frac{(V_{\rm DC} + V_g \sin \omega t)V_g \sin \omega t}{2V_{\rm DC} L_g f_s}\\ \triangle i_{\rm gn3} &= -\frac{V_+ V_g \sin \omega t}{V_{\rm DC} L_g f_s}\\ \triangle i_{\rm gn4} &= -\frac{(V_{\rm DC} + V_g \sin \omega t)V_g \sin \omega t}{2V_{\rm DC} L_g f_s}.\end{aligned} \tag{45}$$

Let $\frac{d\triangle i_{\rm gn1}}{dt} = 0$, then the two solutions are $\sin \omega t = -1$ and $\sin \omega t = -\frac{V_-}{2V_g}$. Then, the maximum value of the $\triangle i_{\rm gn1}$ is

$$\triangle i_{gn1\max} = \frac{(V_- - V_g)V_g}{V_{\rm DC} L_g f_s} \tag{46}$$

when $V_- \geqslant 2V_g$ and is

$$\triangle i_{\rm gn1max} = \frac{V_-^2}{4V_{\rm DC} L_g f_s} \tag{47}$$

when $V_- \leqslant 2V_g$.

The maximum of $\triangle i_{\rm gn2}$ is achieved when $\sin \omega t = -1$ at

$$\triangle i_{gn2\max} = \frac{(V_{\rm DC} - V_g)V_g}{2V_{\rm DC} L_g f_s} \tag{48}$$

and the maximum of $\triangle i_{\rm gn3}$ is achieved when $\sin \omega t = -1$ at

$$\triangle i_{gn3\max} = \frac{V_+ V_g}{V_{\rm DC} L_g f_s}. \tag{49}$$

3) Selection of the Grid Inductor L_g: According to the above analysis, it is clear that the maximum switching ripples of i_g, i.e., the largest one among (39)–(42) and (46)–(49), depend on V_+ and V_-. After careful comparison, it can be found that, when $V_+ \geqslant V_-$, (49) is the largest one and hence, the maximum switching ripple of the grid current is given as

$$\triangle i_{g\max} = \frac{V_+ V_g}{V_{\rm DC} L_g f_s}. \tag{50}$$

On the other hand, when $V_+ \leqslant V_-$, (39) is the largest one and, therefore, the maximum ripple is

$$\triangle i_{g\max} = \frac{V_- V_g}{V_{\rm DC} L_g f_s}. \tag{51}$$

In other words, the maximum grid-current ripple is

$$\triangle i_{g\max} = \frac{\max\{V_+, V_-\}V_g}{V_{\rm DC} L_g f_s}. \tag{52}$$

For a given $\triangle i_{g\max}$, the minimum inductance required is

$$L_g \min = \frac{\max\{V_+, V_-\}V_g}{V_{\rm DC} \triangle i_{g\max} f_s}. \tag{53}$$

4) Comparison With the Conventional RECTO: The switching ripple of the grid current in the conventional RECTO is

$$\begin{aligned}\triangle i_g^{'} &= \frac{\frac{V_-}{V_{\rm DC}} V_{\rm DC} + V_g \sin \omega t}{L_g f_s} d_2\\ &= \frac{1}{L_g f_s V_{\rm DC}}(V_+ V_- - V_g^2 \sin^2 \omega t)\\ &\quad + \frac{(V_+ - V_-)V_g}{L_g f_s V_{\rm DC}} \sin \omega t.\end{aligned} \tag{54}$$

In order to extract the maximum value of the $\triangle i_g^{'}$, let

$$\begin{aligned}\frac{d\triangle i_g^{'}}{dt} &= \frac{-2\omega V_g^2 \sin \omega t \cos \omega t}{L_g f_s V_{\rm DC}}\\ &\quad + \frac{\omega(V_+ - V_-)V_g}{L_g f_s V_{\rm DC}} \cos \omega t\\ &= 0\end{aligned} \tag{55}$$

which means either $\cos \omega t = 0$ or $\sin \omega t = \frac{V_+ - V_-}{2V_g}$. For sure, $\cos \omega t = 0$ is always achievable. However, $\sin \omega t = \frac{V_+ - V_-}{2V_g}$ is only valid when $|V_+ - V_-| \leqslant 2V_g$.

When $|V_+ - V_-| \geqslant 2V_g$, the maximum value of $\triangle i_g^{'}$ is achieved when $\cos \omega t = 0$ at

$$\triangle i_{g\max}^{'} = \frac{V_+ V_- - V_g^2 + |V_+ - V_-|V_g}{L_g f_s V_{\rm DC}}. \tag{56}$$

The switching ripple of the grid current is reduced because

$$\begin{aligned}\frac{\triangle i_{g\max}^{'}}{\triangle i_{g\max}} &= \frac{\frac{V_+V_- - V_g^2 + |V_+ - V_-|V_g}{L_g f_s V_{\rm DC}}}{\frac{\max\{V_+, V_-\}V_g}{V_{\rm DC}L_g f_s}} \\ &\geqslant \frac{V_+V_- + V_g^2}{\max\{V_+,\, V_-\}V_g} \\ &> \frac{V_+V_-}{\max\{V_+,\, V_-\}V_g} \\ &> 1. \end{aligned} \tag{57}$$

When $|V_+ - V_-| \leqslant 2V_g$, the maximum value of the $\triangle i_g^{'}$ is achieved when $\sin\omega t = \frac{V_+ - V_-}{2V_g}$ at

$$\triangle i_{g\max}^{'} = \frac{V_{\rm DC}}{4L_g f_s}. \tag{58}$$

The switching ripple of the grid current is reduced in this case as well because

$$\begin{aligned}\frac{\triangle i_{g\max}^{'}}{\triangle i_{g\max}} &= \frac{V_{\rm DC}^2}{4\max\{V_+,\, V_-\}V_g} \\ &= \frac{2V_+V_- + V_+^2 + V_-^2}{4\max\{V_+,\, V_-\}V_g} \\ &\geqslant \frac{4V_+V_-}{4\max\{V_+,\, V_-\}V_g} \\ &> 1. \end{aligned} \tag{59}$$

C. Power Semiconductor Switches

Moving the neutral point from the midpoint of the split capacitor as in the conventional RECTO to the midpoint of switches Q_3 and Q_4 does not change the voltage stress and the current stress of the switches. Hence, the selection of the switches remains unchanged. However, the equivalent switching frequency in the grid current is increased in the improved RECTO, although the four switches are operated at the same switching frequency. This helps reduce the switching ripple in the grid current if the same grid inductor is used. Because of the same switching frequency of switches, the resulted switching losses should be almost the same for the two RECTO.

VI. Experimental Validation

The improved RECTO was experimentally implemented on a prototype in the laboratory, which is constructed with insulated-gate bipolar transistors controlled by TMS320F28335 DSP. The sampling frequency is $4\,$kHz and the switching frequency is $19\,$kHz. The system parameters used for experiments are the same as those given in Table II. Unbalanced loads and capacitors are applied to demonstrate the robustness of the system against parameter variations.

For the later presented experiments, the current ratings of the 2.2 mH neutral inductors should be around 5 A and 0.2 A, respectively, for the conventional and proposed RECTO. In practice, because of limited available components in the laboratory, two 1.1 mH inductors rated in 10 A and two 1.1 mH inductors rated in 0.5 A are connected in series to form the required 2.2 mH neutral inductors used in the conventional and proposed RECTO, respectively. The used 1.1 mH inductors are shown in Fig. 10. In detail, the size of the neutral inductor used in the conventional RECTO is $5.1 \times 2.5 \times 5.5\,\text{cm}^3$, whereas the one in the proposed RECTO is $0.7 \times 0.7 \times 0.8\,\text{cm}^3$. Clearly, the size of the inductors is significantly reduced by 155 times from 70 to $0.45\,\text{cm}^3$. For fair, it is worth mentioning that this number can vary for different system parameters but the minimum reduction is at least nine times in theory because the inductor current is reduced at least three times for any cases.

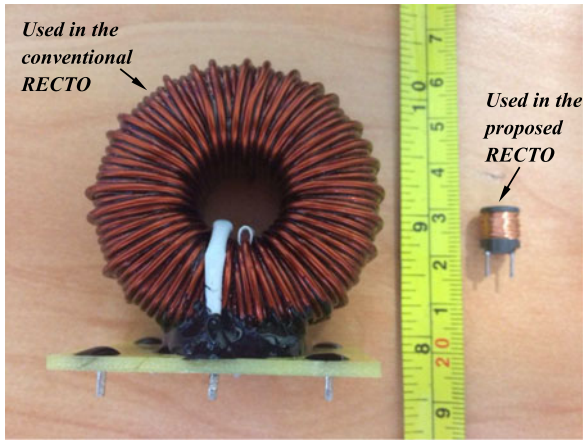

Fig. 10. Size comparison of neutral inductors used in the conventional (left inductor) and improved (right inductor) RECTO.

A. Steady-State Performance

As shown in Fig. 11, the improved RECTO can work well under different V_+ and V_-. For example, the grid current is well controlled to be clean and in phase with the grid voltage when $V_+^* = 200$ V and $V_-^* = 250$ V, as shown in Fig. 11(a). Similar performance can be found in Fig. 11(b) and (c) when $V_+^* = 200$ V and $V_-^* = 200$ V and when $V_+^* = 250$ V and $V_-^* = 200$ V, respectively. According to the recorded experimental data, the power factor is always above 0.99.

B. Transient Performance

Fig. 12 shows the transient responses of the improved RECTO under three scenarios. The first one is a reference change of the voltage V_- from 200 to 250 V, and then back to 200 V, with $R_+ = 470\,\Omega$, $R_- = 470\,\Omega$, and $R = 1470\,\Omega$. As shown in Fig. 12(a), it only took about 280 ms and 160 ms for the two step changes, respectively.

The second scenario is a change of the load R_- from 1940 to $470\,\Omega$, and then back to $1940\,\Omega$. Fig. 12(b) shows that the voltage V_- does not have noticeable overshoot and the transient responses only took about 240 ms and 280 ms, respectively, due to the load changes.

The third scenario is system startup. It is clear that, as shown in Fig. 12(c), the voltages V_+ and V_- were quickly built up to their references, which are 200 V and 250 V, respectively, without large overshoots. The whole startup process took about 360 ms. The grid current was smoothly increased to charge the

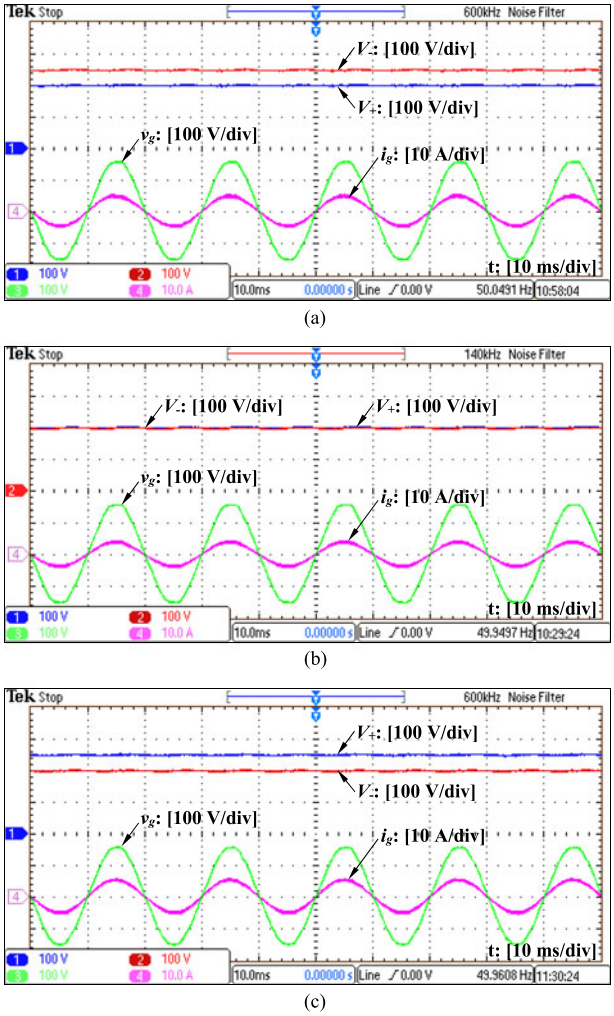

Fig. 11. Steady-state performance when (a) $V_+^* = 200$ V and $V_-^* = 250$ V; (b) $V_+^* = 200$ V and $V_-^* = 200$ V; and (c) $V_+^* = 250$ V and $V_-^* = 200$ V.

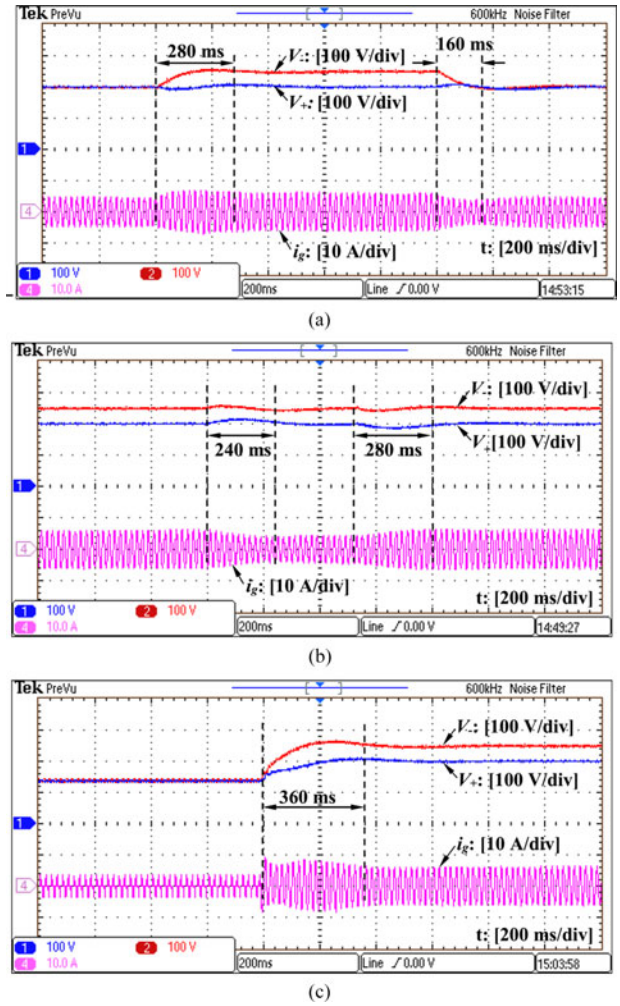

Fig. 12. Transient performance: (a) to a step change of the reference V_-; (b) to a step load change; and (c) during system startup.

capacitors C_+ and C_- at the beginning of the startup process and then was controlled to reach its steady-state value.

C. Comparison With the RECTO Proposed in [6]

In order to clearly demonstrate the reduction of the current stress and the switching ripples of the grid current, the results from the two rectifiers are shown in the left column and the right column of Fig. 13, respectively, for the conventional RECTO and the improved RECTO. As shown in Fig. 13(a), the neutral inductor current i_L of the improved RECTO is much smaller. In order to compare the average values of the two currents, Fig. 13(b) shows the current i_L after applying a 6 kHz filter to exclude high-frequency components. The maximum absolute values of the inductor current are around 4.82 A and 0.19 A, respectively. Therefore, the inductor current is reduced by about $\frac{4.82}{0.19} \approx 25$ times in the improved RECTO, which is consistent with the theoretical analysis. Because of the different currents carried by the neutral inductor, the voltage across the inductor v_{L_N} (excluding high-frequency components) is a dc component with a fundamental ac component in the conventional RECTO, while it is a pure dc component in the proposed RECTO as shown in Fig. 13(b).

Fig. 13(c) shows the voltage v_{AN}. In the conventional RECTO, it changes between $V_+ = 250$ V and $-V_- = -250$ V, which means the conventional RECTO is operated similar to a half-bridge converter. However, the voltage v_{AN} in the improved RECTO changes between 0 and $V_{\mathrm{DC}} = 450$ V during the positive half cycle and between 0 and $-V_{\mathrm{DC}} = -450$ V during the negative half cycle. As a result, the improved RECTO is operated similarly to a full-bridge converter, which matches with the theoretical analysis in Fig. 7.

In order to verify the switching operation of the RECTO, a few switching periods of the current i_g are chosen and shown in Fig. 13(d). In theory, the maximum switching ripple of the i_g is achieved when $\sin \omega t = 1$ for the improved RECTO. As a result, the chosen periods are around the peak of i_g. On the other hand, the maximum switching ripple in the conventional RECTO is the higher one between (56) and (58). According to the system parameters given in Table II, (58) is higher, which is achieved when $\sin \omega t = \frac{V_+ - V_-}{2V_g} \approx -0.16$. As a result, the chosen periods for the conventional RECTO are around the point where $\sin \omega t = -0.16$. It can be found that the maximum switching ripple of the grid current in the proposed RECTO is 1.04 A, whereas it is 1.35 A in the conventional RECTO. Their theoretical values are 1.03 A and 1.34 A, respectively,

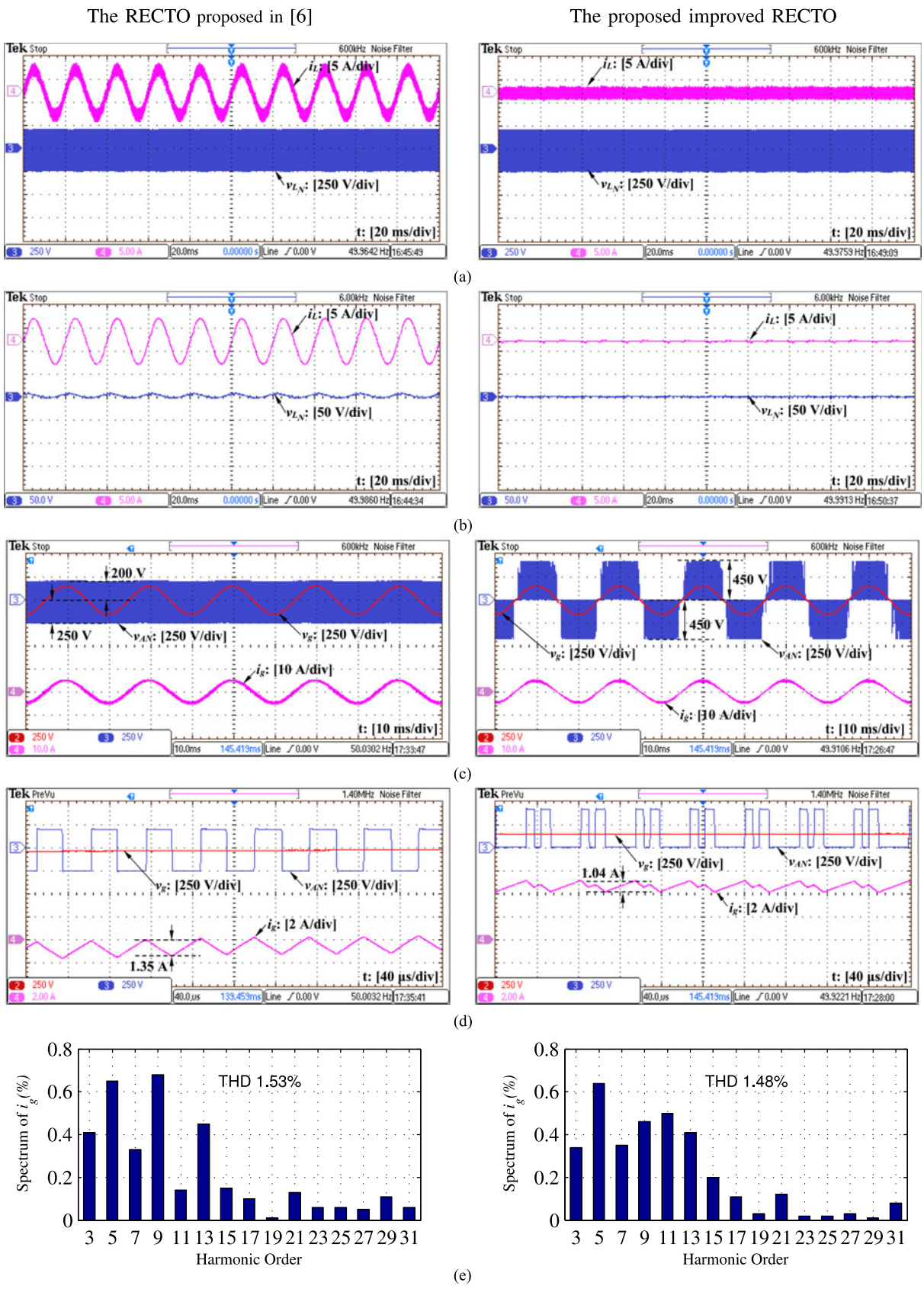

Fig. 13. Experimental results when $V_+^* = 200$ V and $V_-^* = 250$ V: (a) inductor current i_L and the voltage v_{L_N}; (b) inductor current i_L and the voltage v_{L_N} with a 6 kHz filter applied; (c) voltages $v_{\rm AN}$, v_g, and the grid current i_g during a few fundamental periods; (d) voltages $v_{\rm AN}$, v_g, and the grid current i_g during a few switching periods during which the ripple of the grid current reaches its maximum value; and (e) harmonic spectrum of the grid current i_g.

according to (50) and (58). As a result, both values well match the theoretical analysis. Importantly, the switching ripple of the grid current is indeed reduced, here, by $\frac{1.35}{1.04} \approx 1.3$.

The harmonic distribution of the grid current i_g is shown in Fig. 13(e) according to the recorded experimental data from a Yokogawa WT1600 power analyzer. The total harmonic distortion (THD) of i_g is slightly improved from 1.53% to 1.48%.

VII. Conclusion

In this paper, the conventional RECTO has been improved to reduce the neutral and grid inductors, by moving the neutral inductor away from the path of the grid current. In this case, only the current difference of the dual loads flows through the neutral inductor, which is much smaller than the grid current. Accordingly, the current stress of the neutral inductor can be significantly reduced. In theory, the inductor current-stress and size can be reduced by at least three times and nine times, respectively. For the given example, the inductor current-stress is reduced by about 25 times. This also changes the operation modes and modulation strategy of the RECTO as well, which helps reduce the grid inductor for the same switching ripple. Considering the reduced neutral inductor, the power density of the improved RECTO is improved. Note that the voltage, current stress of the switches, and the other features of the conventional RECTO, e.g., two outputs and unity power factor, are not affected. Experimental results have validated the theoretical analysis.

For future research, the following issues will be explored to further optimize the performance of the improved RECTO: 1) The equivalent switching frequency on the grid inductor is increased in the improved RECTO, which helps reduce the switching-frequency ripples in the grid current. However, the effect of the increased equivalent frequency on differential EMI needs to be explored. It is expected that a discrete high-frequency model will be built in order to analyze and compare the differential EMI for the conventional and improved RECTO. 2) Because of the change of the neutral inductor, the currents carried by the four switches and also the neutral inductor have been changed. Since the current carried by the neutral inductor is significantly reduced, the power loss of the neutral inductor is expected to be reduced. However, more systemically research on power losses of each switch and inductor should be conducted to confirm the efficiency performance of the improved RECTO. Soft switching/three-level techniques may be considered to reduce power losses.

Acknowledgment

The authors would like to thank the reviewers for their insightful and interesting comments, which have helped the authors significantly improve the quality of this paper.

References

[1] Q.-C. Zhong and T. Hornik, *Control of Power Inverters in Renewable Energy and Smart Grid Integration*. New York, NY, USA: Wiley, 2013.

[2] W.-L. Ming, Q.-C. Zhong, and X. Zhang, "A single-phase four-switch rectifier with significantly reduced capacitance," *IEEE Trans. Power Electron.*, vol. 31, no. 2, pp. 1618–1632, Feb. 2016.

[3] R. Machado, S. Buso, and J. Pomilio, "A line-interactive single-phase to three-phase converter system," *IEEE Trans. Power Electron.*, vol. 21, no. 6, pp. 1628–1636, Nov. 2006.

[4] D. Dong, I. Cvetkovic, D. Boroyevich, W. Zhang, R. Wang, and P. Mattavelli, "Grid-interface bidirectional converter for residential DC distribution systems—Part one: High-density two-stage topology," *IEEE Trans. Power Electron.*, vol. 28, no. 4, pp. 1655–1666, Apr. 2013.

[5] D. Dong, F. Luo, X. Zhang, D. Boroyevich, and P. Mattavelli, "Grid-interface bidirectional converter for residential DC distribution systems—Part 2: AC and DC interface design with passive components minimization," *IEEE Trans. Power Electron.*, vol. 28, no. 4, pp. 1667–1679, Apr. 2013.

[6] W.-L. Ming and Q.-C. Zhong, "A single-phase rectifier having two independent voltage outputs with reduced fundamental frequency voltage ripples," *IEEE Trans. Power Electron.*, vol. 30, no. 7, pp. 3662–3673, Jul. 2015.

[7] R. Srinivasan and R. Oruganti, "A unity power factor converter using half-bridge boost topology," *IEEE Trans. Power Electron.*, vol. 13, no. 3, pp. 487–500, May 1998.

[8] Y.-K. Lo, T.-H. Song, and H.-J. Chiu, "Analysis and elimination of voltage imbalance between the split capacitors in half-bridge boost rectifiers," *IEEE Trans. Ind. Electron.*, vol. 49, no. 5, pp. 1175–1177, Oct. 2002.

[9] Y.-K. Lo, C.-T. Ho, and J.-M. Wang, "Elimination of the output voltage imbalance in a half-bridge boost rectifier," *IEEE Trans. Power Electron.*, vol. 22, no. 4, pp. 1352–1360, Jul. 2007.

[10] J. C. Salmon, "Circuit topologies for single-phase voltage-doubler boost rectifiers," *IEEE Trans. Power Electron.*, vol. 8, no. 4, pp. 521–529, Oct. 1993.

[11] X. Zhang and C. Gong, "Dual-buck half-bridge voltage balancer," *IEEE Trans. Ind. Electron.*, vol. 60, no. 8, pp. 3157–3164, Aug. 2013.

[12] C. Liu and J.-S. Lai, "Low frequency current ripple reduction technique with active control in a fuel cell power system with inverter load," *IEEE Trans. Power Electron.*, vol. 22, no. 4, pp. 1429–1436, Jul. 2007.

[13] X. Li *et al.*, "Power management unit with its control for a three-phase fuel cell power system without large electrolytic capacitors," *IEEE Trans. Power Electron.*, vol. 26, no. 12, pp. 3766–3777, Dec. 2011.

[14] J.-I. Itoh and F. Hayashi, "Ripple current reduction of a fuel cell for a single-phase isolated converter using a DC active filter with a center tap," *IEEE Trans. Power Electron.*, vol. 25, no. 3, pp. 550–556, Mar. 2010.

[15] R.-J. Wai and C.-Y. Lin, "Active low-frequency ripple control for clean-energy power-conditioning mechanism," *IEEE Trans. Ind. Electron.*, vol. 57, no. 11, pp. 3780–3792, Nov. 2010.

[16] W.-L. Ming and Q.-C. Zhong, "Single-phase voltage-doubler with mismatched capacitors for balanced output voltages and reduced DC-bus voltage ripples," in *Proc. IEEE Energy Convers. Congr. Expo.*, 2013, pp. 4830–4836.

[17] Q.-C. Zhong, J. Liang, G. Weiss, C. Feng, and T. Green, "H^∞ control of the neutral point in 4-wire 3-phase DC–AC converters," *IEEE Trans. Ind. Electron.*, vol. 53, no. 5, pp. 1594–1602, Nov. 2006.

[18] T. Hornik and Q.-C. Zhong, "Parallel PI voltage–H^∞ current controller for the neutral point of a three-phase inverter," *IEEE Trans. Ind. Electron.*, vol. 60, no. 4, pp. 1335–1343, Apr. 2013.

[19] H. Kim and K.-H. Kim, "Filter design for grid connected PV inverter," in *Proc. IEEE Int. Conf. Sustain. Energy Technol.*, Nov. 2008, pp. 1070–1077.

[20] D. Dong, F. Luo, D. Boroyevich, and P. Mattavelli, "Leakage current reduction in a single-phase bidirectional AC–DC full-bridge inverter," *IEEE Trans. Power Electron.*, vol. 27, no. 10, pp. 4281–4291, Oct. 2012.

[21] W.-L. Ming and Q.-C. Zhong, "Current–stress reduction of the neutral inductor in a rectifier with two outputs," in *Proc. 2016 IEEE Energy Convers. Congr. Expo.*, Sep. 2016.

[22] A. K. Ziarani and A. Konrad, "A method of extraction of nonstationary sinusoids," *Signal Process.*, vol. 84, no. 8, pp. 1323–1346, Apr. 2004.

[23] A. Tilli and A. Tonielli, "Sequential design of hysteresis current controller for three-phase inverter," *IEEE Trans. Ind. Electron.*, vol. 45, no. 5, pp. 771–781, Oct. 1998.

[24] T. Hornik and Q.-C. Zhong, "A current control strategy for voltage-source inverters in microgrids based on H^∞ and repetitive control," *IEEE Trans. Power Electron.*, vol. 26, no. 3, pp. 943–952, Mar. 2011.

[25] A. Bento, E. da Silva, and E. dos Santos, "Reducing the inductor size and current stress by interleaved bidirectional boost rectifiers used for power factor correction," in *Proc. IEEE 21st Annu. Appl. Power Electron. Conf. Expo.*, 2006, pp. 273–279.

Qing-Chang Zhong (M'03–SM'04–F'17) photograph and biography not available at the time of publication.

Wen-Long Ming (M'16) photograph and biography not available at the time of publication.